The Simulation and Analysis of a Single and Double Inverted Pendulum with a Vertically-Driven Pivot

Group 7: Gustavo Lee

Abstract— The inverted pendulum is a simple system in which both stable and unstable configurations are easily observed. The upward inverted state is unstable, though it has long been known that a simple rigid pendulum can be stabilized against small disturbances in its inverted state by oscillating its pivot in an up-and-down motion. Numerical simulations of the inverted pendulum are employed to investigate the stable and unstable domains of the system with respect to the excitation amplitudes and frequencies. The associated basins of attractions, extracted by interpolated cell mapping, are fractal.

I. INTRODUCTION & MOTIVATION

The inverted pendulum was originally investigated by P. L. Kapitza, a prominent Russian physicist and Nobel laureate. At that time, the inverted pendulum and the larger phenomenon of dynamical stability was all but unknown to the majority of physicists at the time. On the subject, Kapitza had this to say:

> "...the striking and instructive phenomenon of dynamical stability of the turned pendulum not only entered no contemporary handbook on mechanics but is also nearly unknown to the wide circle of specialists..." [1]

> "...not less striking than the spinning top and as instructive." [1]

Since then, however, the inverted pendulum has been a widely studied problem not only in mechanics, but also in control theory. It is often one of the first problems introduced in Mechanics and Controls textbooks. Variations of this problem include using PID controllers, neural networks, or fuzzy control to stabilize the pendulum. Another way to stabilize the inverted pendulum that does not require control theory is a simple vertically oscillating pivot. Within a range of excitation amplitudes and frequencies, the pendulum may be stabilized. If the pivot is driven by a simple harmonic motion, the pendulum's motion is described by the Mathieu equation.

II. THEORY

A. Single Inverted Pendulum: N=1

The single pendulum consists of a solid rod (a rectangular piece, in our case) attached to an oscillating pivot, about which the rod is free to rotate, as shown in Figure 1. In Figure 1, the pendulum is depicted as a massless rod of length ℓ attached to a particle mass m at its end. The derivation of the equations of motion begin with the Lagrangian. With the position of the inverted pendulum with an oscillatory base
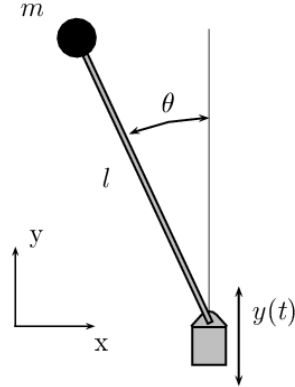

Fig. 1. Diagram of an Idealized Pendulum in its Inverted State

given by $(\ell \sin \theta, y + \ell \cos \theta)$ and the velocity, or derivative of this position with respect to time, given by $v^2 = \dot{y}^2 + 2\ell\dot{\theta}\dot{y}\sin\theta + \ell^2\dot{\theta}^2$, the Lagrangian for the system is readily given by Equation 1.

$$\mathcal{L} = \frac{m}{2}(\ell^2\dot{\theta}^2 + \dot{y}^2 + 2\ell\dot{\theta}\dot{y}\sin\theta) - mg(y(t) + \ell\cos\theta) \quad (1)$$

where θ describes the angle between the pendulum arm and the upward vertical in the counterclockwise direction, $\dot{\theta}$ describes the derivative of θ with respect to time, m is the mass of the pendulum, ℓ is the length of the pendulum (or as is the case in our experiments, the effective length when the pendulum is not an idealized massless rod), and finally, g is the acceleration due to gravity. Solving this first order Lagrangian in $\dot{\theta}$ and θ by the equation

$$\frac{\mathrm{d}}{\mathrm{d}t}\frac{\partial\mathcal{L}}{\partial\dot{\theta}} - \frac{\partial\mathcal{L}}{\partial\theta} = 0 \quad (2)$$

and re-scaling, or non-dimensionalizing, we arrive at

$$\ddot{\theta} + (\beta f(\tau) - \alpha)\sin\theta = 0 \quad (3)$$

where $\ddot{\theta}$ is the second derivative of θ now with respect to non-dimensional time: $\tau = \omega t$, ω is the driving frequency of the oscillating pivot, and the scaled dimensionless parameters are $\alpha = g/\ell\omega^2, \beta = b/\ell$, and $f(\tau)$ corresponds to the normalized driving function, such that $\partial_\tau^2 y(t) = bf(\tau)$. This second-order system can be generalized to include damping terms as such:

$$\ddot{\theta} + \gamma\zeta(\dot{\theta}) + (\beta f(\tau) - \alpha)\sin\theta = 0 \quad (4)$$

where γ represents a constant, scaled, friction coefficient and ζ is some function on the angular velocity $\dot\theta$.

B. Linear Stability Analysis

For the inverted pendulum system, there are two fixed points given by:

$$(\theta^*, \dot\theta^*)_- = (\pi, 0) \tag{5}$$

$$(\theta^*, \dot\theta^*)_+ = (0, 0) \tag{6}$$

With no oscillatory motion, it's clear the inverted position is unstable and the downward position stable. However, the stability of each respective fixed point can be changed by varying the excitation amplitude and frequency of the oscillating pivot base. Making the local transformation,

$$\eta_\pm = \theta^*_\pm + \delta\theta_\pm \tag{7}$$

we finally arrive at the Mathieu equation[2].

$$\delta\ddot\theta_\pm \mp (\beta f(\tau) - \alpha)\delta\theta_\pm = 0 \tag{8}$$

The Mathieu equation approximates the motion of the pendulum quite well, especially when the amplitude of oscillations are small. Note that the stability of the fixed point is determined by the sign of the linear prefactor, and that should $y(t)$ be an eigensolution of the operator ∂_τ^2 with eigenvalue $-\omega^{-2}$, the stability of the fixed points are not determined by the sign of β as $-\beta$ corresponds to a phase shift of π relative to β. A study on the stability of the inverted state within the excitation amplitude and frequency parameter space performed by Blackburn et al [3] shows that the inverted state is stable as long as the frequency and amplitude of the oscillating pivot were within the following two curves,

$$\epsilon = \sqrt{2}/\Omega \tag{9}$$

$$\epsilon = 0.450 + 1.799/\Omega^2 \tag{10}$$

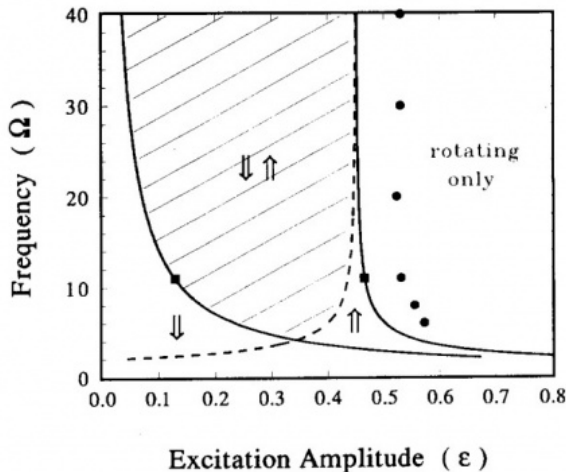indicated by the shaded region in Figure 2. The up and down

Fig. 2. Stability Diagram for the Pendulum

arrows signify regions of stability for the regular and inverted

positions of the pendulum. The diagram indicates that the inverted state of the pendulum is achieved at higher excitation amplitudes, but also that all stability is lost at both fixed points above a critical excitation amplitude, during which the pendulum exhibits continuous rotating motion. The forcing frequency Ω and the forcing amplitude ϵ in the diagram are defined as

$$\Omega = f/f_0 \tag{11}$$

$$\epsilon = \frac{A\omega_0^2}{g} \tag{12}$$

where f is the frequency in Hz, f_0 is the natural frequency of the pendulum, A is the amplitude in meters, ω_0 is the natural frequency in rad/s, and g is the acceleration due to gravity in m/s^2.

C. Effective Energy Potential

Simulation and experimentation will later show that stability for the single inverted pendulum can easily be achieved. For every excitation amplitude (ϵ) and frequency (ω), there exists a maximum critical angle of release (θ_c) for which the system reverts to its stable inverted state at $\theta = 0$. Essentially, the more stable the system is, the larger this θ_c will be. This stability boundary between instability and stability can be seen in Figure 2. It is the exponentially decaying line to the left of the shaded region. In essence, as we move further into the shaded region by increasing our excitation amplitude, we are make the inverted state more stable, thereby increasing θ_c. This is illustrated by Figure 3.
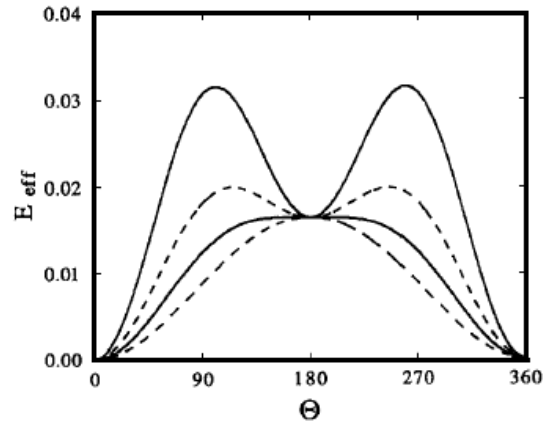
Fig. 3. Effective Energy Potential

First and foremost, the illustration shows that there are two stable fixed points at $\theta = 0, \pi$, noting that in this case the stable up position is $\theta = \pi$ and the stable down position is $\theta = 0$, not to be confused with our original definitions. At low excitation amplitdues, the stable-down fixed point is "more stable" than the stable up position. The small hump shows that as the inverted position becomes stable, it resides at a higher potential than the stable down position. In the initial stages, this hump is quite flat and any perturbation in the system will provide it with enough energy to roll off the hump. As the excitation amplitude is increased, the well

created by the energy potential becomes deeper. As a result, more energy is required to overcome the hump and larger perturbations are necessary to knock the pendulum from the stable inverted state.

D. Double Inverted Pendulum: N=2

The double pendulum is essentially two single pendulums attached end-to-end. The motion of the double pendulum is governed by a set of coupled ordinary differential equations shown below.

$$\ddot{\theta}_1 = -\frac{a_1 + a_2 - a_3}{2L_1(m_2\sin(\theta_1-\theta_2)^2 + m_1)} \tag{13}$$

$$\ddot{\theta}_2 = \frac{b_1 + b_2 + b_3}{2L_2(m_2\sin(\theta_1-\theta_2)^2 + m_1)} \tag{14}$$

where,

$$a_1 = m_2(L_1\dot{\theta}_1{}^2\sin(2\theta_1 - 2\theta_2) + 2L_2\dot{\theta}_2{}^2\sin(\theta_1 - \theta_2)) \tag{15}$$

$$a_2 = g((2m_1 + m_2)\sin\theta_1 + m_2\sin(\theta_1 - 2\theta_2)) \tag{16}$$

$$a_3 = \ddot{y}((2m_1 + m_2)\sin\theta_1 + m_2\sin(\theta_1 - 2\theta_2)) \tag{17}$$

$$b_1 = L_2 m_2\dot{\theta}_2{}^2\sin(2\theta_1 - 2\theta_2) \tag{18}$$

$$b_2 = (m_1+m_2)(2L_1\dot{\theta}_1{}^2\sin(\theta_1-\theta_2)+g(\sin(2\theta_1-\theta_2)-\sin\theta_2)) \tag{19}$$

$$b_3 = \ddot{y}(m_1 + m_2)(\sin\theta_2 - \sin(2\theta_1 - \theta_2)) \tag{20}$$

As Figure 4 shows, the equations of motion derived correspond to the double derivatives of θ_1 and θ_2, which are the angles in the counterclockwise direction from the vertical (as indicated). Much like the inverted pendulum, the double
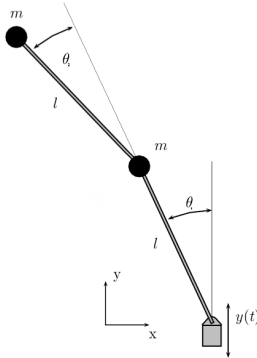

Fig. 4.   Diagram of an Idealized Double Pendulum in its Inverted State

inverted pendulum is inherently unstable. By oscillating the base at high enough excitation amplitudes, the system can be stabilized. Its dynamics are much more complicated than the single inverted pendulum. The trajectory of the end mass can be irregular and may not display periodicity or symmetry about the vertical axis and will often exhibit chaotic behavior.

III. SIMULATION

A. Modeling in Matlab

Before any experiments were performed, the single and double inverted pendulums were simulated using the equations of motion found in the previous section. Simulation was done in Matlab using Simulink. As you can see from Figure 5, the model for the single inverted pendulum circulates $\ddot{\theta}$, integrating once to obtain $\dot{\theta}$ and then again to obtain θ, from which the x and y positions of the pendulum tip are calculated. A sin wave of frequency ω and amplitude A is added to the position of the pivot. Lastly, a frictional damping term is added, as results will later show that frictional damping, not viscous, was present in the experimental set-up of the system. The output parameters of the simulation are x, y, θ, and $\dot{\theta}$, from which phase portraits and other plots can be obtained.
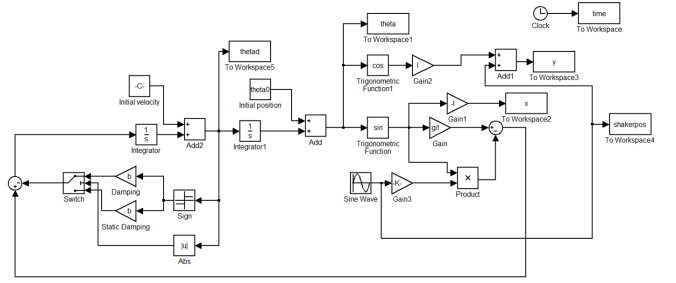

Fig. 5.   Simulink Model of the Single Pendulum

The model for the double inverted pendulum is very similar to the single pendulum, only a bit more complex. Figure 6 shows the Simulink model for the double inverted pendulum.
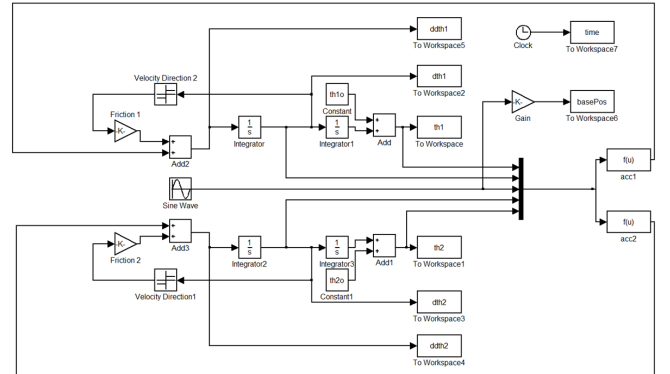

Fig. 6.   Simulink Model of the Double Pendulum

IV. EXPERIMENTAL SETUP

A. Materials

- Oscillating base
- Rod or pendulum simulacrum
- Reflective tracking material
- Camera

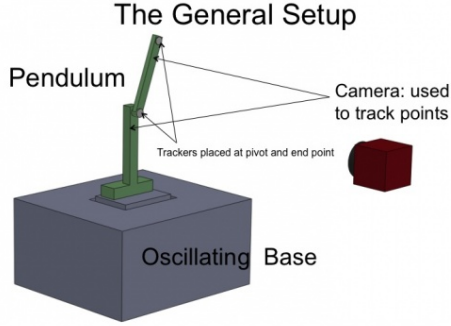The general setup with the aforementioned materials is illustrated in Figure 7.

Fig. 7.   General Setup of the Inverted Pendulum Experiment

B. Camera Setup

For the purpose of gathering critical information about the actual motion of the pendulum when subjected to an harmonically driven pivot, the group used two cameras and various methods of tracking. The first camera that was used was a PointGrey high speed camera running at a maximum of 200 frames per second (fps). It communicated via firewire to the computer. With this setup, tracking was done in real-time with LabView. The biggest advantage to this method was that the LabView software was readily available and significantly reduced the amount of time required to acquire the position data from the video capture. However, actual frame rate times varied from frame to frame due to real-time calculations, which had to be taken into account later during data analysis. Furthermore, this method was not quite feasible for the double pendulum experiments when the movement of the pendula was much quicker and more erratic, obscuring the tracking point.

The second camera used was a MotionXtra high speed camera running at 1000 fps. This camera alleviated all problems associated with the first camera, but required post-processing methods to obtain usable data. Videos were saved on the camera, then later transferred to a computer, allowing for capture of faster motions and requiring offline point tracking in Matlab. Figure 8 shows the two cameras.

Fig. 8.   Motion Xtra camera running at 1000 fps (left); PointGrey camera running at 200 fps (right)

C. Tracking with Matlab

Using the high-speed cameras and LabView to track the pendula was no easy task. At the very beginning of each tracking session, a group member selected the coodinates of the search area, from which the tracking program searched to find the centroid of the tracker in the image. The trackers that we used were blotches of white-out against a black electrical tape background, as well as 10mm white plastic balls super-glued to black electrical tape. Additionally, a black backdrop was sometimes necessary for additional contrast between anything in the camera's image view and the point to be tracked. Next, we set the threshold data to determine a good 0-255 grayscale value to distinguish between white tracker pixels and darker non-tracker pixels. Each pixel now constituted a binary value of true or false. Then, based on the search area grid initally selected, the program averages the locations of all the "true" points to get the position of the centroid of the tracker pixels. This centroid is then used as the updated search point for the next frame. Using this algorithm, the program was able to successfully track data points, which was then used to obtain relevant data. However, many times the search grid would lose the tracking points, particularly when they were obscured from the view of the camera. This problem was exacerbated for the double pendulum when certain portions of the tracking point for one pendulum, such as the pivot, was covered up by the other pendulum. This problem was sometimes circumvented using a clever scheme of adding a constraint to the position of the pivot: that it only moves in the vertical direction. Then the position of the hidden pivot could be calculated using the position of the end of the pendulum and the length of the pendulum. Other times, brute force and manual tracking on a frame by frame basis was necessary.

D. The Oscillating Base

The oscillating base is the device used to vertically shake the pivot of the pendulum. It consists of a function generator, amplifier, motor, air bearing, accelerometer, and oscilloscope. The function generator creates a sine wave at the desired frequency. However, the amplitude of this signal is not powerful enough to drive the motor in the base. Thus, the signal is passed through an amplifier that adds current and increases the amplitude of the signal, which is then sent to the motor. The motor converts this current into a force and is allowed to move vertically with near frictionless motion via air bearings. An accelerometer attached to the motor sends a signal to the oscilloscope in order to provide valuable feedback about the precise amplitude provided by the entire mechanical system. The amplitude is provided through the output peak to peak voltage of the signal, which can then be converted into actual displacement amplitude by

$$A_{disp} = \frac{9.8 \cdot V_{pk}/2 \cdot 10}{(2\pi \cdot \omega)^2} \tag{21}$$

where ω is the excitation frequency and V_{pk} is the peak to peak voltage provided by the oscilloscope.

Figure 9 depicts this process. The red arrow shown on the oscilloscope shows the peak to peak voltage that is used to ultimately calculate the actual displacement amplitude.
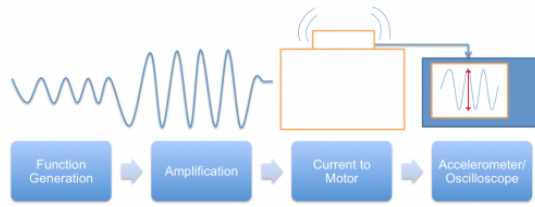
Fig. 9.   Schematic of the Entire Oscillating Base Mechanism

E. Pendulum Configuration - Single

1) Original Schematic: When the experiments first began, the set-up shown in Figure 10 was used.
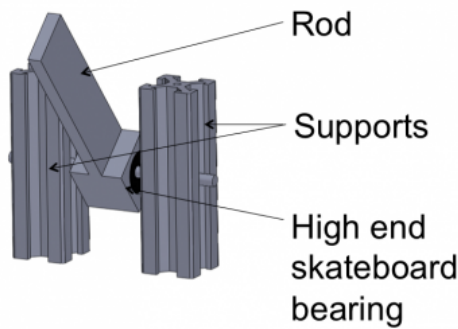

Fig. 10.   Original Schematic of the Single Pendulum

In this set-up, the effective length of the aluminum pendulum was 6.9 cm. The pendulum's pivot consisted of two high-end ball bearings used for skateboard wheels placed side-by-side. The pivot and its bearings were attached to an axle that had supports on both ends. This set-up, however, had two critical problems. First, the effective length of the pendulum was too large. With such a long pendulum made of heavy material, the mechanical set up of the oscillating base could not provide stability beyond a small range of frequency values, thereby rendering the experiment quite ineffective. Second, the two side-by-side ball bearing configuration created strange frictional behavior in the system. At small amplitudes of oscillation, the pendulum would rapidly settle either to the left or to the right of the vertical up position. The rotation of the pendulum about the axis appeared to have a notch, an unwanted effect of this bearing configuration. This notched behavior is illustrated in Figure 11, which shows the pendulum, as it loses energy, initially seems to settle at the inverted position, but instead settles in a slightly offset position.

2) Modified Schematic: To alleviate some of the problems with the original set-up of the pendulum, a new simpler set-up was created. The new set-up only had one support and one ball-bearing and most importantly, it was shortened significantly to an effective length of 3.1 cm (shown in Figure 12).

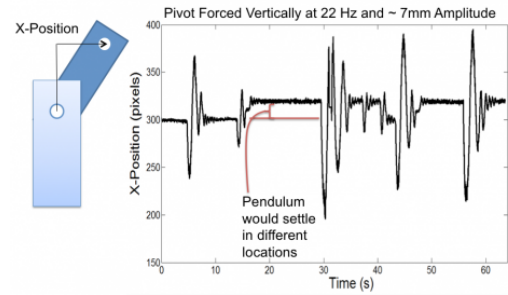This shorter, lighter pendulum was more manageable in

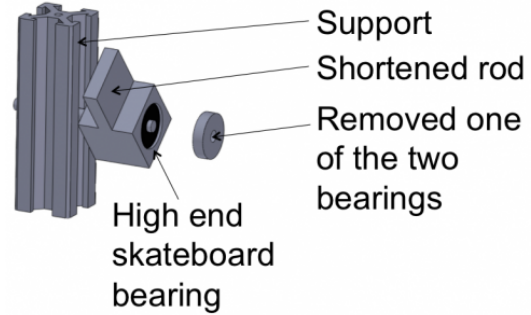Fig. 11.   Offset Problem with the Original Single Pendulum

Fig. 12.   Modified Schematic of the Single Pendulum

terms of stability. Also, the notch initially present in the ball bearings was visibly reduced, though it did not completely fix the problem. But, as Figure 13 shows, the new set-up greatly improved the behavior of the pendulum, allowing damping data to be obtained with sufficient accuracy. The data shows a geometric decay of amplitude from one period to the next, indicating fricitional damping, as opposed to viscous damping. This effect will be discussed more later.
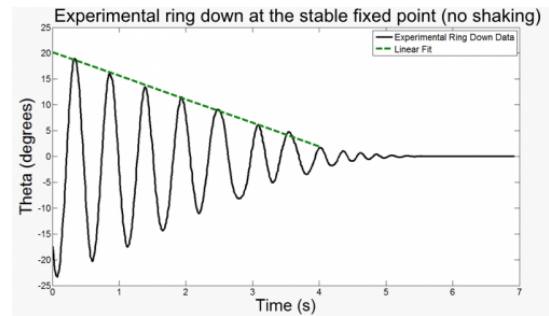

Fig. 13.   Amplitude Decay of Modified Single Pendulum

F. Pendulum Configuration - Double

The double pendulum set-up, shown in Figure 14 was built using Lego pieces clamped to a support. The effective length of each pendulum was 3.2 cm. This set-up did not require the use of bearings, as the Lego pieces with holes simply rotated about thin Lego rods. The light weight of the system allowed the inverted state to stabilize rather easily for a wide range of excitation amplitudes and frequencies. Upon

experimentation using this set-up, our group soon realized the superiority of using extremely light-weight Lego pieces. This was a double-edged sword, however. Because the pieces were so lightweight and not rigidly attached, the Lego pieces would rotate in and out of the plane of rotation, causing an unwanted degree of freedom. Furthermore, the set-up would occasionally break and scatter due to its light-weight, unsturdy frame.
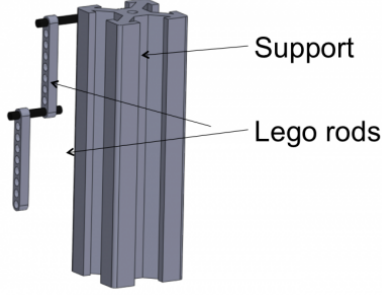

Fig. 14.   Schematic of the Double Pendulum

V. Results

A. Determination of the Damping Parameter

The damping parameter was determined by tracking the pendulum in its stable down position with no oscillatory motion applied to the base. The pendulum was released at an arbitrary angle and tracked until it nearly came to rest.
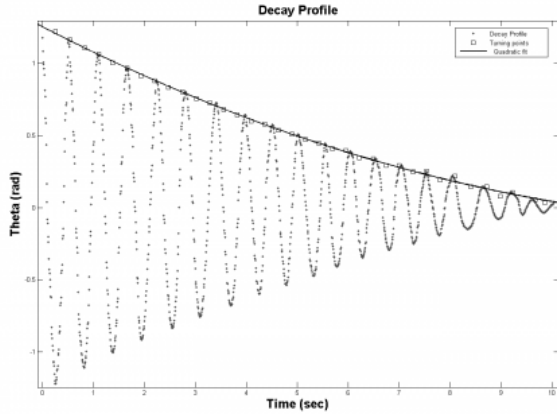

Fig. 15.   Decay Profile of the Single Pendulum

Figure 15 shows the trajectory of θ_n as a time-series. From the profile of the series, it is possible to determine, implicitly, the form of the damping in the dynamics of the single pendulum system, shown by Equation (4). A second-order polynomial in t,

$$f(t; a, b, c) = at^2 + bt + c \qquad (22)$$

was used for approximating the profile (also shown in Figure 15). The fit converged with an RMSE value of 0.006664, with parameter values determined to be $a = 0.0082 \pm$

$0.000687, 95\%$, $b = -0.1979 \pm 0.0054, 95\%$, $c = 1.28 \pm 0.009, 95\%$. Since $|a/b| \approx \vartheta(|b|/10)$, we can be confident that the decay profile is linear, and the damping is therefore frictional [4].

Now that the type of damping has been determined, the actual damping parameter can be determined by fitting the the first period of the decay profile of the single pendulum to a sine wave. This is used to first determined the natural frequency of the pendulum, which analytically describes an initial condition of the system. In Figure 16, an explicit Euler numeric method was used to integrate the dynamics of the system and compare the time-series output to the experimentally determined data.
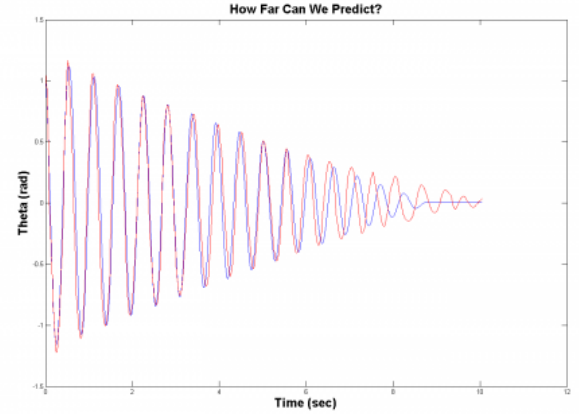

Fig. 16.   Damping Parameter Fit to Experimental Data

The damping parameter is then determined variationally, by a minimization of the RMSE of the two series with equal weighting. Using this method, the damping coefficient, from Equation (1), is determined to be $\gamma \approx 2.5$. Figure 16 shows the comparison of the two time-series. The two time-series appear to match quite well and diverge only after 6 to 7 periods.

B. Stability Map from Experimental Data

Using the damping coefficient, the single and double pendulum Simulink models can accurately produce theoretical models of the actual set-up, as long as the other parameters (ie. effective length, mass, and acceleration due to gravity, excitation amplitude and frequency) reflect actual values from experimental data.

A stability map, much like Figure 2 can be created from the Simulink simulation by sweeping through all viable frequencies and obtain the minimum excitation amplitude to maintain stability when the system is given a slight perturbation. This frequency vs. amplitude mapping provides a parameter space, which illustrates which areas are stable and/or unstable for the both the inverted-up and normal-down positions. Figure 17 shows the theoretical stability curve for frequencies from 0 Hz to 40 Hz and their respective amplitudes. Note that this figure is very similar to Figure 2. Moreover, a stability map was also found using experimental
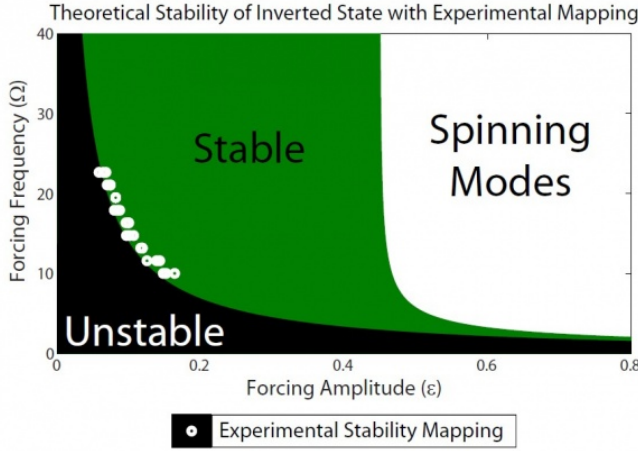
Fig. 17. Theoretical and Experimental Stability Curve

data for comparison. Since all the experimental parameter values were used for the simulation, one would expect the theoretical and experimental stability maps to appear very similar, which is indeed the case. However, with the limited capacity of the set-up of the system, only frequencies from 15 Hz to 35 Hz were feasible. Figure 17 shows the experimental stability curve data points as white dots overlayed over the theoretical curve obtained from the simulations.

C. Effective Potential

The presence of the effective potential was definitely existent in the experimental data, as well as the simulation. It can be most prominently observed in Figure 18. The
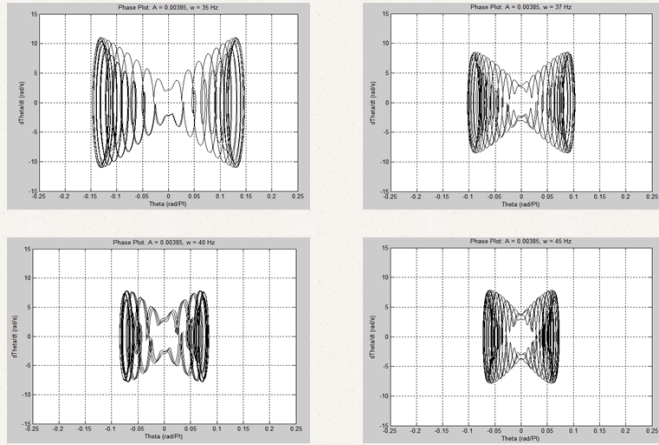

Fig. 18. Phase Plots of the Inverted Single Pendulum for Varying Stabilities

figure shows the phase plots of the system defined with certain parameters that are all the same, with the exception of frequency. The top left phase plot shows the system driven by a 35 Hz forcing function, whereas the bottom right plot shows a single pendulum driven by a 45 Hz forcing function. In other words, the system becomes more stable as the forcing frequency increases, given all other parameters remain the same. In essence, the well of the

effective potential has become deeper and steeper. It can be seen from the 4 phase plots that the system is oscillating about plus or minus 0.12 radians relative to the inverted state at 35 Hz, but only oscillating about plus or minus 0.05 radians at 45 Hz, where the well has become deeper. In this case, the system needs a greater amount of potential energy to overcome this well.

D. Basins of Attraction

From the simulation, we were also able to extract interesting plots of the basins of attractions for the inverted single pendulum system. In order to do this, however, one must take an array of different intial conditions (θ and $\dot{\theta}$) in phase space and record the final position of the trajectory after a certain amount of time for each of the initial conditions. This is easily visualized by assigning a color representing the final angular position to a pixel at the appropriate initial position and velocity coordinates in phase space. In our case, black represents the inverted stable state, $\theta = 0$ and white represents the bottom stable state, $\theta = \pi$. One particular problem that arises is the potential to have a very long simulation run time. For example, to obtain images of the basins of attraction for a pendulum driven by an oscillating pivot of 50 Hz forcing frequency, a reasonable time would be 50 cycles, or 1 second; and the resolution could be a set of 500x500 different initial conditions in the phase space. This would be quite expensive in terms of simulation run time. A way around this problem is to simulate only the first forcing cycle. After the first cycle, a mapping of each individual intial condition as it evolves 1 cycle at a time is obtained. With this mapping, one can use a method called Interpolated Cell Mapping (ICM) to iterate through successive cycles of forcing and get through 1 second of simulation much faster with sufficient accuracy [5]. Figure 19 shows the basins of attraction for a system with the following parameters: $\ell = 2.72$ cm, $g = 9.8$, $\gamma = 10$, $\omega = 50$ Hz, and various amplitudes (0, 2 mm, 3 mm, 4 mm, and 10 mm).
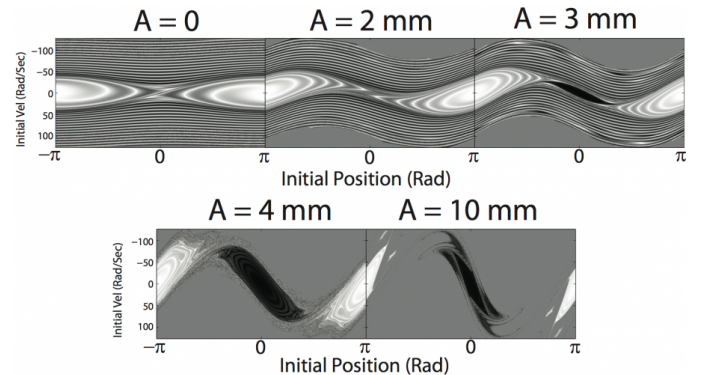

Fig. 19. Basins of Attractions for Various Excitation Amplitudes

As the excitation amplitude increases, the inverted fixed point comes into the stable region around $A = 3$mm and grows rapidly until by $A = 10$mm, we can see that the system is on the verge of entering the rotational portion of its stability map, where both fixed points lose stability. The

large expanses of gray are areas in which the trajectory of those initial conditions eventually mapped to points outside of the visible phase space, and thus, had no mapping and could not be mapped further, even if the trajectory eventually returned.

E. Separable Behavior from Double Pendulum

When studying the double pendulum system being subjected to varying excitation amplitudes and forcing frequencies, an interesting phenomena was observed. It was seen that the double pendulum has 4 fixed points. The inverted vertical up for both pendula, the stable down position for both pendula, stable up for one pendulum with the other stable down and vice versa, the latter two referred to by our group as the "Flipping Modes". Figure 20 shows a phase portrait for the double pendulum being driven at 24 Hz with the inner pendulum in the up state, and the outer pendulum in the down state.
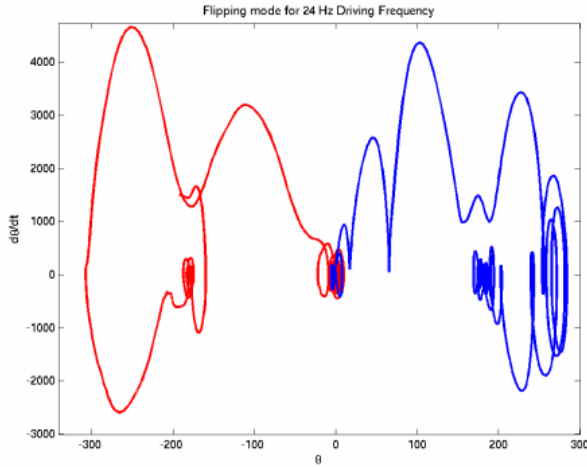

Fig. 20.   Phase Plot of the Flipping Mode at 24 Hz

This anti-symetric state is then perturbed. Upon perturbation, the system now settles in the "flipped" state with the inner pendulum in the down state, and the outer pendulum in the up state. The time series $\theta_{1,n}, \theta_{2,n}$ is illustrated in Figure 21.

The figure shows that one pendulum goes from the stable up position to the stable down position, while the other pendulum does the exact opposite. In other words, the two pendula "flip" states. This suggests the existence of separable dynamics in the anti-symmetric state $(0, \pi), (\pi, 0)$. Since in either of these anti-symmetric states the small-angle approximation is valid, it should be possible to simplify the dynamics of the system treating small perturbations of the inner pendulum as inertial restoring forces on the outer pendulum. This also explains why the symmetric states $(0, 0), (\pi, \pi)$ do not exhibit this phenomenon. Intuitively, the gauge freedom of the potential energy implies that for these symmetry preserving states the position of the inner pendulum simply defines a higher or lower potential level of the outer pendulum for the $\theta_1 = 0$ and $\theta_1 = \pi$ states,
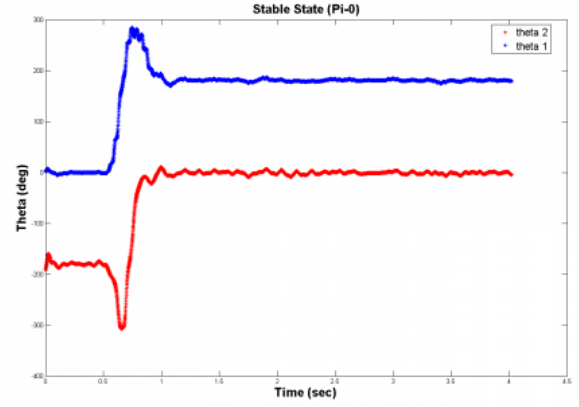

Fig. 21.   Time Series of Each Pendulum in the Double Pendulum

respectively. As long as the symmetry is not broken, the outer pendulum is expected to behave as an independent single pendulum. However, this is only a conjecture and more theoretical work is required.

VI. CONCLUSION

The experimental results suggest that the single pendulum set-up could be built better to maximize the range of frequencies and amplitudes for which an inverted stable up can be observed. Minizing the weight of pendulum can greatly increase the "performance" of the inverted pendulum, as we found out using the make-shift Lego pendulum. Our experimental data matched very closely with theoretical data, indicating that the damping parameter was found correctly to sufficient accuracy. Though the experimental portion was somewhat limited by the mechanical capacities of the system, we were still able to obtain valuable data. All in all, we were able to analyze many aspects of its behavior pertinent to non-linear dynamics.

VII. FUTURE WORK

Future work includes the feasibility of widening the range of frequency and amplitudes of the single pendulum set-up. Further, a stability map of excitation amplitude versus frequency for the double pendulum would be interesting to experimentally and theoretically obtain. And why stop there? A triple pendulum seems quite feasible mechanically, though the complexity of simulation part would increase exponentially with N. Future work also includes studying the period-doubling cascade, resurrection series [6], and chaotic behavior of higher-order pendulum systems.

VIII. ACKNOWLEDGMENTS

REFERENCES

[1] P. L. Kapitza, *Collected papers of P. L. Kapitza*. Pergamon Press, 1965, vol. 2.

[2] G. G. M. V. Bartuccelli and K. V. Georgiou, "On the dynamics of a vertically driven damped planar pendulum," *Proc. R. Soc. Lond.*, vol. 458, pp. 3007–3022.

[3] N. G.-J. James A. Blackburn, H. J. T. Smith, "Stability and hopf bifurcations in an inverted pendulum," *American Journal of Physics*, vol. 60, pp. 903–908.

[4] D. A. A. Marchewka and R. Beichner, "Oscillator damped by a constant-magnitude friction force," *American Journal of Physics*, vol. 72, pp. 477–483.

[5] B. H. Tongue and K. Gu, "Interpolated cell mapping of dynamical systems," *Journal of Applied Mechanics*, vol. 55, pp. 461–466.

[6] P. M. Morse and H. Feshbach, *Methods of Theoretical Physics*. McGraw-Hill, 1953.